Supporting Information: Direct, in operando observation of the bilayer solid electrolyte interphase structure: Electrolyte reduction on a non-intercalating electrode

Christopher H. Lee[a], Joseph A. Dura[b], Amy LeBar[a], Steven C. DeCaluwe[a,*]

[a] *Department of Mechanical Engineering, Colorado School of Mines, Golden, CO 80401, USA*

[b] *NIST Center for Neutron Research, Gaithersburg, MD, 20899, USA*

1. NR Sensitivity Modeling

One major advance of this work is to identify alternative non-intercalating anode materials to improve the neutron reflectometry (NR) sensitivity to the SEI. In our previous publication [1], the Cu electrode had significant SLD contrast with the surrounding layers, which led to a relatively weaker SEI effect on the resulting NR data. A number of alternative non-intercalating electrode chemistries were explored and evaluated for low NR contrast with the substrate and electrolyte SLDs and ease of fabricating a suitable NR sample (dense, low surface roughness, and non-reactive with the Si substrate). Figure S1 shows simulated NR SLD profiles (insets) and corresponding reflectivity (main figures) for three non-intercalating electrodes– Cu (Figure S1(a)), Au (Figure S1(b)), and W (Figure S1(c))–before and after growing the SEI observed in our previous study [1]. Figure S1(a) shows simulated NR similar to our previous study, where the SEI has a rather subtle effect on the NR, due to high SLD contrast. Au (Figure S1(b)) has slightly less SLD contrast and greater change in the NR signal, while W (Figure S1(c)) has very little SLD contrast with the surrounding substrate and electrolyte layers. This corresponds with simulated NR spectra which are qualitatively different in the 'no SEI' and 'SEI' conditions.

2. Tungsten Electrode Fabrication

To optimize the W deposition process, W thin films were prepared on polished, 76.2 mm Si wafers, which were first cleaned using a μ-90[1] detergent scrub, followed by a rinse in millipore DI water and drying *via* blown N_2, and then cleaned with a spin-rinse in HPLC-grade ethanol. Initial reflectivity simulations shown in Figure 1 indicated enhanced NR sensitivity for substrates with the native oxide (SiO_2) removed. Hence the silicon wafers were etched in dilute hydrofluoric acid (HF) prior to deposition, for this portion of the study. Cleaned wafers were installed in a Semicore DC-magnetron sputtering unit with a 99.95% W target, which was pumped to a vacuum of 0.1 μTorr.

Initial deposition attempts optimized the process established by Watjen [2] by varying the Ar chamber pressure and sputtering power. A Tencor P10 profilometer was used to measure film thickness, and sputtering time was adjusted such that all deposited films were approximately 50 nm thick. The samples were then characterized using atomic force microscopy (AFM) on a Veeco Dimension 3100 Atomic Force Microscope

*Corresponding author. Tel: +1-303-273-3666.

Email address: decaluwe@mines.edu (Steven C. DeCaluwe)

[1] Certain commercial equipment, instruments, materials, suppliers, or software are identified in this paper to foster understanding. Such identification does not imply recommendation or endorsement by the National Institute of Standards and Technology, nor does it imply that the materials or equipment identified are necessarily the best available for the purpose.

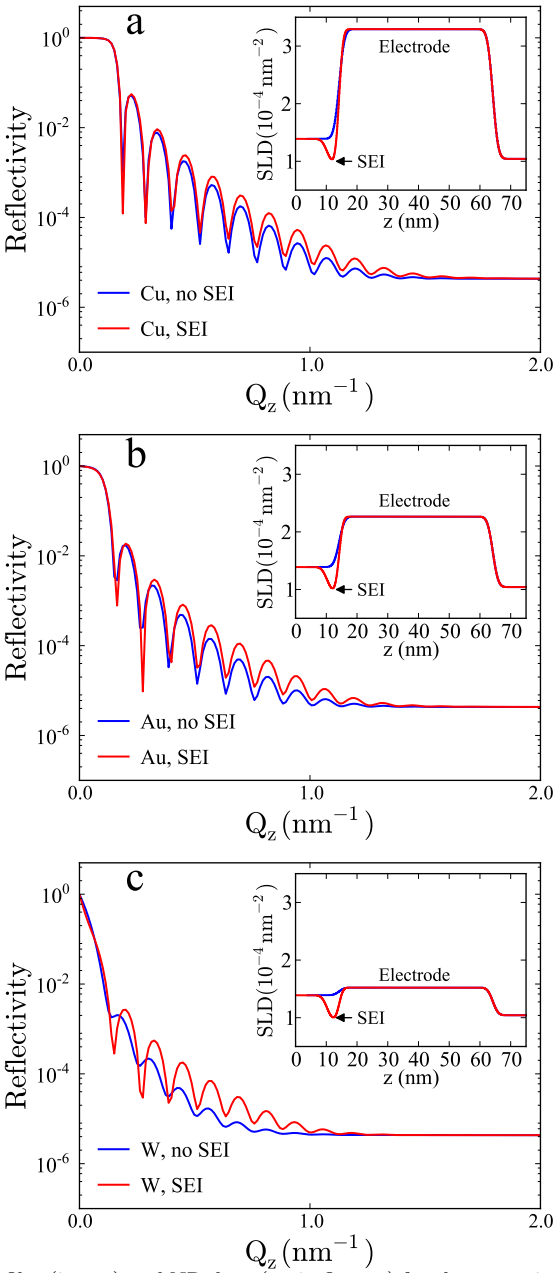

Figure 1: Simulated NR SLD profiles (insets) and NR data (main figures) for three non-intercalating electrodes: (a) Cu; (b) Au; (c) W. The NR sensitivity to the SEI is inversely proportional to the SLD contrast between the electrode and its surrounding layers, making W a particularly sensitive platform for measuring the SEI chemistry and structure.

Table 1: RMS roughness values (nm) measured via AFM for initial tungsten deposition

Power (W)	Ar Pressure (mTorr)		
	5	10	20
50	0.557	0.443	0.486
100	0.812	0.852	1.12
200	1.29	0.732	0.581

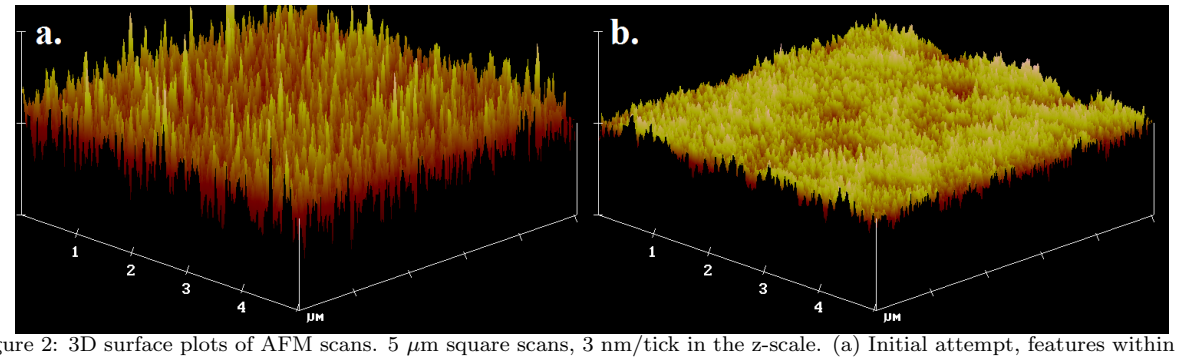

Figure 2: 3D surface plots of AFM scans. 5 μm square scans, 3 nm/tick in the z-scale. (a) Initial attempt, features within the 3-4 nm range; (b) Optimized attempt, features under 2 nm.

with Bruker TESP-V2 probes. The AFM scans were done in tapping mode over 5 μm squares at a scan rate of 0.2 Hz.

Table 1 shows the RMS roughness values (nm) measured by AFM for the initial range of deposition conditions. AFM measured a minimum RMS roughness of 0.443 nm for 50 W power and 10 mTorr Ar pressure. The sample was then characterized by x-ray reflectivity (XRR) on a Bruker D8 X-ray Reflectometer at the NIST Center for Neutron Research (NCNR) in Gaithersburg, MD. The data were reduced using ReflPak software [3], and fit using the differential evolution algorithm in the Refl1d software package, developed at the NCNR, in collaboration with the University of Maryland [4]. Despite the low roughness reported by AFM, the XRR-measured roughness was 6 nm, which is unacceptable for NR. As the incident x-ray beam used in XRR is 1 mm thick and probes the entire surface of the 76.2 mm wafer, the increased roughness in XRR vs. AFM is therefore suspected to be from larger features that were not visible through AFM.

As lower deposition rates typically result in smoother films, the sputtering power and pressure were lowered for the second round of depositions. Table 2 shows the AFM-measured RMS roughness values (nm) for each deposition process. The roughness values are noticeably lower than those in the first optimization attempt. Figure 2 compares the AFM scans for the initial (Figure 2(a)) and final (Figure 2(b)) deposition rounds. The best sample in the second round (Figure 2(b)), deposited under 15 W power and 3 mTorr Ar pressure, shows much smaller features than that from the first round (Figure 2(a)). This sample was then characterized using XRR. Figure 3 shows the XRR results for this optimized sample, including the XRR data and best fit (Figure 3(a)) and fitted SLD profile (Figure 3(b)). Throughout this document, numbers in brackets represent 68% confidence intervals and error bars and $\pm$ uncertainties represent one standard

Table 2: RMS roughness values (nm) measured via AFM for optimized tungsten deposition

Power (W)	Ar Chamber Pressure (mTorr)			
	1	3	5	10
10	0.280	0.358	0.367	0.497
15	0.426	0.224	0.326	0.314

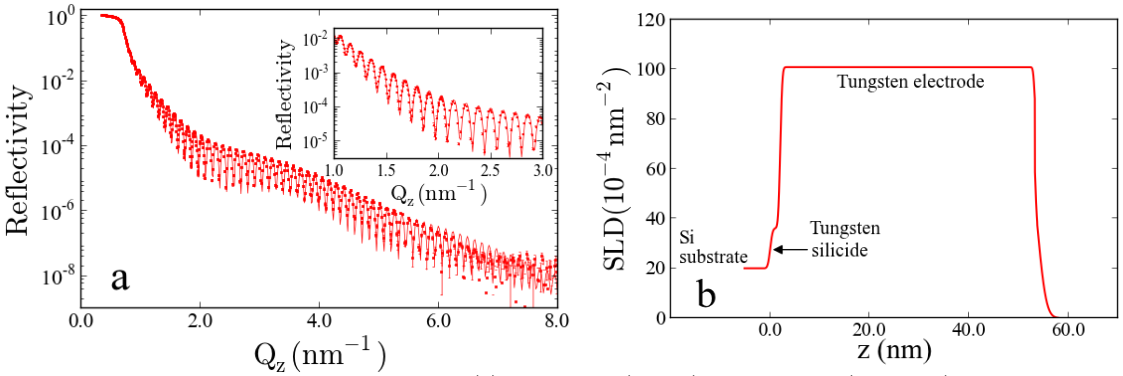

Figure 3: XRR results for optimized W thin film. (a) XRR data (points) with best fit (solid line). Inset is zoomed in to highlight the quality of the fit; (b) X-Ray SLD profile for best fit. Results show high-quality reflectivity out to high Q and a fitted RMS roughness of 1.4 nm.

error. Results confirm the suitable roughness (RMS roughness = 1.4 nm) and W density, and demonstrate excellent reflectivity data quality (high signal-to-noise) out to very high angles, which will enable greater NR sensitivity for the nm-thin SEI layer.

Finally, with the W deposition routine optimized, a thermal oxide was grown as a substrate on the Si wafer. The thermal oxide served as a barrier to prevent Li intercalation into the Si support and to prevent formation of any unknown tungsten silicides during sputtering (as observed in Figure 3). Any such unintended layers would introduce additional uncertainty into the NR fitting, thereby reducing the ability to quantify the chemical structure of the SEI. The silicon wafers used as working electrode substrates were first RCA cleaned then thermally oxidized at 900°C for 23 minutes in a dry O_2 atmosphere (at a flowrate of 3000 sccm) to form an approximately 10 nm thick oxide layer. Variable angle spectroscopic ellipsometry measurements were made at multiple locations on the wafer in a raster pattern to confirm the uniformity of the oxide.

3. Alternative NR Fits

Herein, we present alternative models which were fit to the data in the main manuscript, but which were determined inferior to those fits. A range of the models fit simultaneously to data sets 'W_{bare}' and 'W_{SEI}' are shown in Figure 4. The models employ varying numbers of layers for the substrate (thermal SiO_2 plus tungsten), and varying numbers of layers at the tungsten free surface (e.g., tungsten oxide for 'W_{bare}' and SEI for 'W_{SEI}'). For models with varying numbers of layers and therefore varying numbers of fitting parameters, the Bayesian Information Criterion (BIC) must be used to differentiate between the goodness-of-fit between the various models. A BIC difference greater than 6 between two fits presents a strong case for rejecting the fit with the higher BIC. [5]

On the basis of the BIC, the model shown in Figure 4(a) was selected as the best fit. Even though the fits in Figures 4(e) and (f) provided lower BIC values, these models were deemed infeasible due to the two-layer thermal SiO_2 structure identified. Repeated NR measurements on identically-grown SiO_2 / W layers only ever identified a single SiO_2 substrate layer.

Similarly, Figure 5 shows a range of models fit to the 'W_{elyte}' data. The lowest BIC value was for a model with the 2-layer 'pre-SEI' at the tungsten-electrolyte interface (Figure 5(a)). Note that Figure 5(d), which has a 3-layer pre-SEI at the tungsten free surface, gives a roughly equivalent fit to the data, which is statistically indistinguishable from that chosen as the 'best fit.'

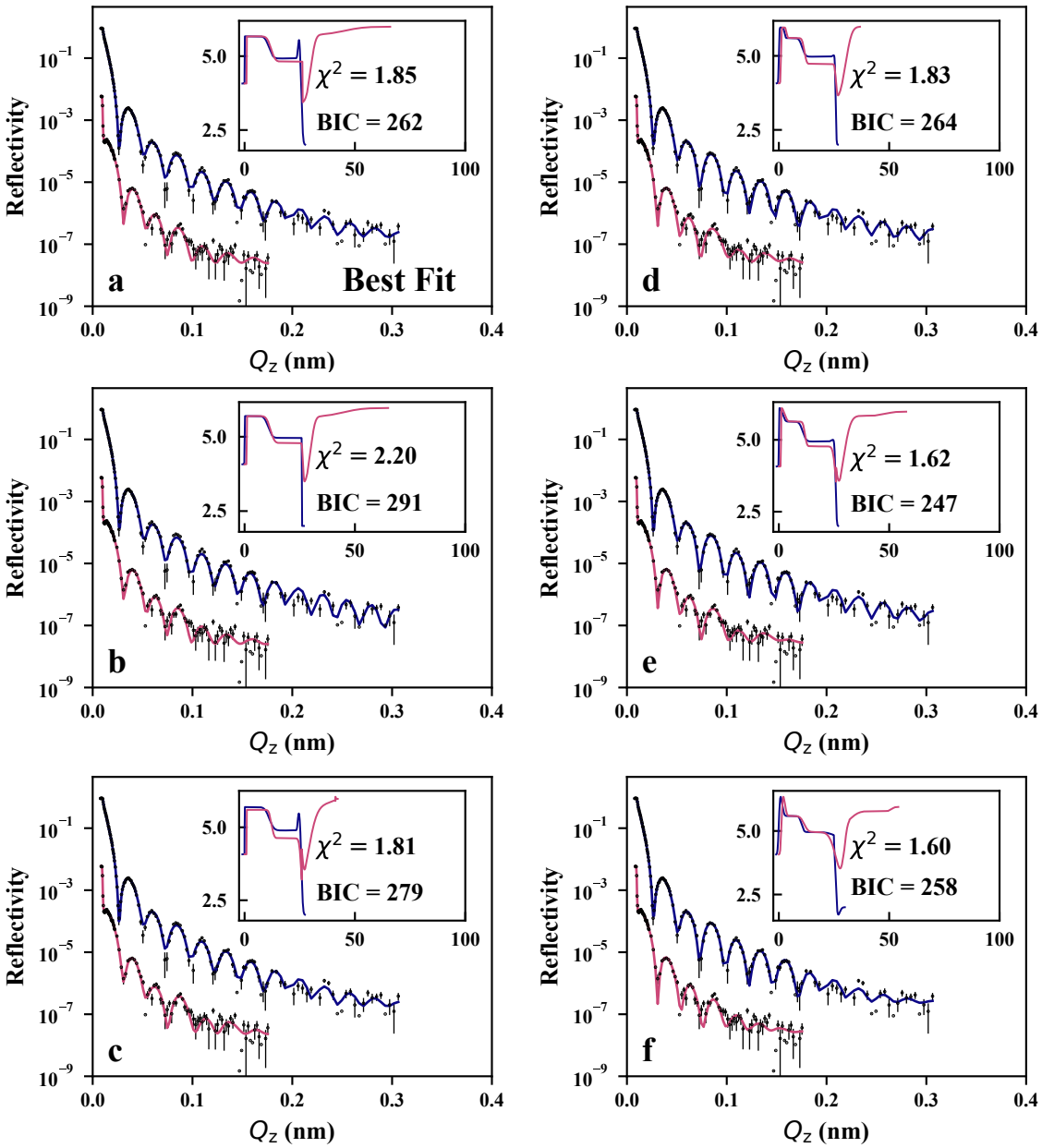

Figure 4: Simultaneous fits to 'W_{bare}' and 'W_{SEI}'. Models have varying numbers of layers at the tungsten free surface. On the basis of BIC, (a) was deemed the best model. While the fits in (e) and (f) have lower BIC values, repeated measurements on similarly grown thermal oxides did not reproduce the 2-layer SiO2 structure identified in those fits.

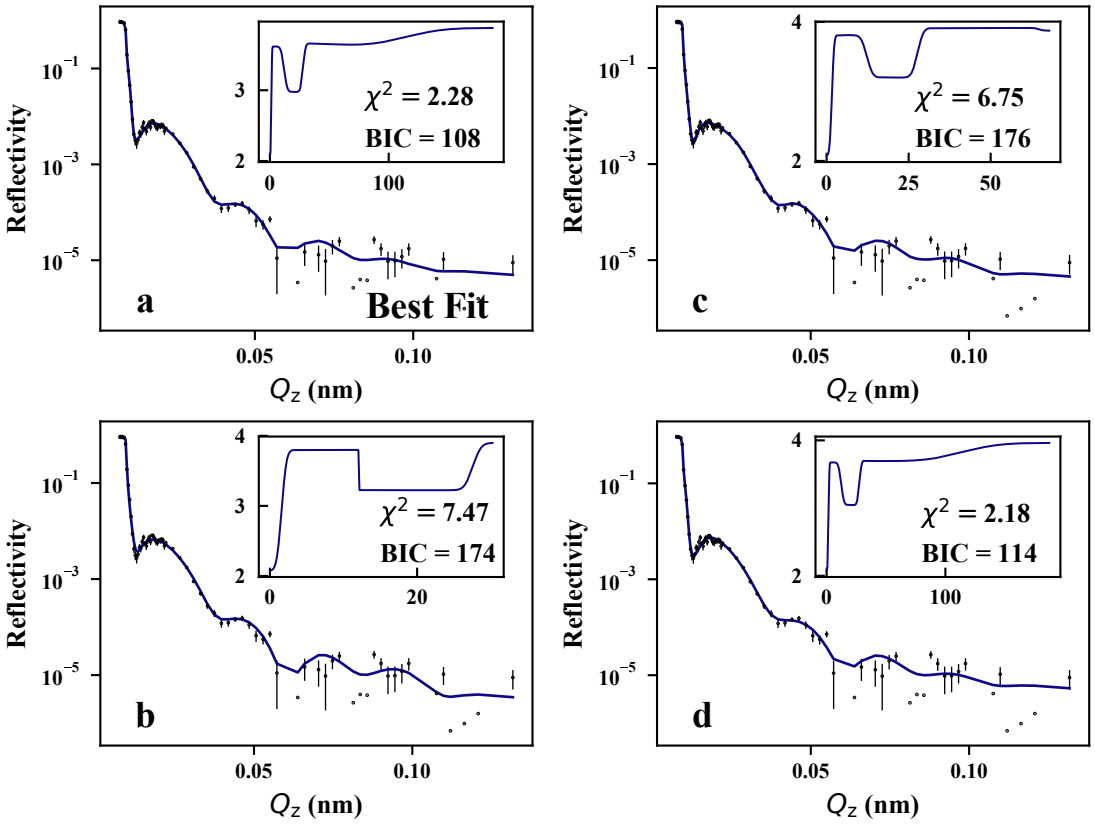

Figure 5: NR fits to 'W_{elyte}' data. Models have varying numbers of layers at the tungsten free surface. On the basis of BIC, (a) was deemed the best model. The fit in (d) also provides a suitable fit.

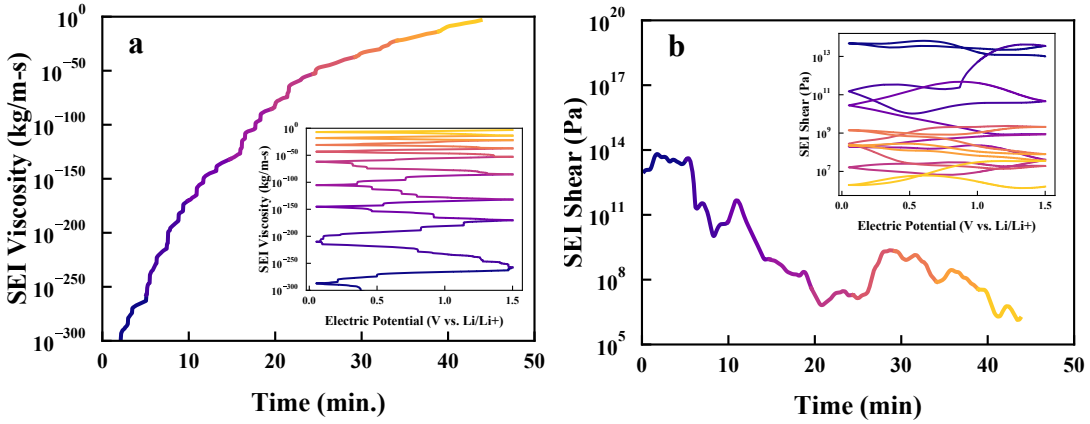

Figure 6: SEI visco-elastic properties from EQCM-D data. (a) Viscosity; (b) Shear. Results demonstrate a layer that grows more rigid during CV cycling. Insets show visco-elastic properties as a function of tungsten electrode potential. No notable trends as a function of electric potential are observed.

4. QCM Viscoelastic Properties

Figure 6 presents the visco-elastic information reported by the EQCM-D fits, including the viscosity (Figure 6(a)) and the shear (Figure 6(b)). Neither parameter showed any systematic variation with cycle number or voltage (see insets), but rather evolved primarily as a function of time. The viscosity increased monotonically, in a relatively continuous manner, while the shear generally decreased as a function of time, but did so in a rather noisy, non-monotonic manner. Both parameters indicate an SEI that grew more rigid, as a function of time.

5. References

[1] J. E. Owejan; J. P. Owejan; S. C. DeCaluwe; J. A. Dura. Solid electrolyte interphase in li-ion batteries: Evolving structures measured in situ by neutron reflectometry. *Chem. Mater.*, 24(11):2133–2140, 2012.

[2] J.I. Watjen; T.J. Bright; Z.M. Zhang; C. Muratore; A.A. Voevodin. Spectral radiative properties of tungsten thin films in the infrared. *Int. J. Heat Mass Transf.*, 61:106–113, 2013.

[3] P.A. Kienzle, K.V. O'Donovan, J.F. Ankner, N.F. Berk, and C.F. Majkrzak. Reflpak: 1-d reflectometry reduction and analysis. http://www.ncnr.nist.gov/reflpak.

[4] P. A. Kienzle, J. A. Krycka, and N. Patel. Refl1d: Interactive depth profile modeler. Available from: http://www.reflectometry.org/danse/software.

[5] R.E. Kass and A.E. Raftery. Bayes factors. *J. Am. Stat. Assoc.*, 90(430):773–795, 1995.